RSC Advances

PAPER

View Article Online
View Journal | View Issue

Cite this: *RSC Adv.*, 2025, **15**, 28601

2-[2,6-Bis(4,4′-difluorobenzhydryl)-4-methylphenylimino]-3-aryliminobutylnickel complex precatalysts tuning polyethylene elastomers with different molecular weights

Dongzhi Zhu,[ab] Qiuyue Zhang,[b] Dedong Jia,[b] Yanping Ma[b] and Wen-Hua Sun*[b]

A series of 2-[2,6-bis(4,4′-difluorobenzhydryl)-4-methylphenylimino]-3-aryliminobutylnickel complexes was synthesized and fully characterized using FT-IR, elemental analysis, and single-crystal X-ray diffraction in the case of **Ni1**. The structural analysis revealed significant deviation from ideal tetrahedral geometry. When activated with MAO, these complexes demonstrated superior catalytic performance compared to previously reported unsymmetrical 2,3-bis(arylimino)butylnickel analogs. The optimized system, incorporating *ortho*-difluorobenzhydryl and *para*-methyl electron-donating groups, achieved an exceptional activity of 26.56 × 10^6 g(PE) mol^{-1} (Ni) h^{-1}. The resulting polyethylenes exhibited a broad spectrum of microstructures, ranging from semi-crystalline to nearly amorphous, with unimodal ultra-high molecular weights (M_w: 4.33–26.72 × 10^5 g mol^{-1}) and tunable branching degrees (62–200/1000 C) achieved through a controlled chain-walking mechanism. The unique balance of molecular weight and crystalline-amorphous regions in these polymers translated to outstanding mechanical properties, including tensile strengths of 1.68–13.42 MPa, elongations at break of 388–529%, and elastic recoveries of 21–73%. Notably, the **Ni1**/Et_2AlCl catalyst system demonstrated enhanced thermal stability for ethylene polymerization, achieving a higher activity of 2.56 × 10^6 g(PE) mol^{-1} (Ni) h^{-1} at 90 °C compared to 1.94 × 10^6 g(PE) mol^{-1} (Ni) h^{-1} at 70 °C for **Ni1**/MAO. However, the polymers produced with **Ni1**/Et_2AlCl exhibited lower molecular weights (2.67–10.90 × 10^5 g mol^{-1}) and inferior mechanical properties, underscoring the critical role of molecular weight in determining material properties.

Received 24th June 2025
Accepted 30th July 2025

DOI: 10.1039/d5ra04501k

rsc.li/rsc-advances

Introduction

Polyethylene elastomers (PEEs),[1–4] being produced *via* ethylene feedstock, have recently garnered significant attention as useful materials. They can offer a compelling combination of elasticity, chemical resistance, and processability, characteristics that are on par with those of thermoplastic elastomers (TPEs).[5–10] Structurally, PEEs are characterized by their flexible backbones incorporating diverse branching architectures (*e.g.*, short-chain and long-chain branches), and perform the properties similar to those of polyolefin elastomers (POEs), which are commonly produced through the copolymerization of ethylene and α-olefins.[11–22] Beyond facilitating more economical process without costly α-olefins, PEEs with different microstructures could be tailored *via* the adjustable chain-walking mechanisms by modified α-diimine–nickel complex precatalysts in conjunction with optimal polymerization parameters, ultimately controlling their distinctive elastomeric properties.[23–33]

Pioneered by Brookhart group utilizing α-diimine Pd/Ni precatalysts for branched polyethylenes,[23] the concerted effort has been made in extensively modifying such model catalysts, primarily focusing on developing substituents on the *N*-aryl moieties as well as new model complexes.[2,33] Through finely tuning steric hindrance and electronic effects of ligands for the nickel complexes, the catalytic performances have been gradually improved including better thermostability and higher activities,[2,33] meanwhile the resultant polyethylenes are simultaneously enhanced for useful properties.[1,33]

Notably, the unsymmetrical configuration of ligands has significantly enhanced the performances of their nickel complexes,[33] stabilizing active species and controlling resultant polyethylenes with high branching degrees (exceeding 100/1000 C).[34–36] The systematic investigations of bis(arylimino)acenaphthene (**A–B**, Scheme 1)[34–47] and 2,3-bis(arylimino)butyl (**C–D**, Scheme 1)[48–51] have been explored by employing bulky

[a]*Guangxi Key Laboratory of Advanced Structural Materials and Carbon Neutralization, School of Materials and Environment, Guangxi Minzu University, Nanning 530105, China*

[b]*Key Laboratory of Engineering Plastics and Beijing National Laboratory for Molecular Sciences, Institute of Chemistry, Chinese Academy of Sciences, Beijing 100190, China. E-mail: whsun@iccas.ac.cn*

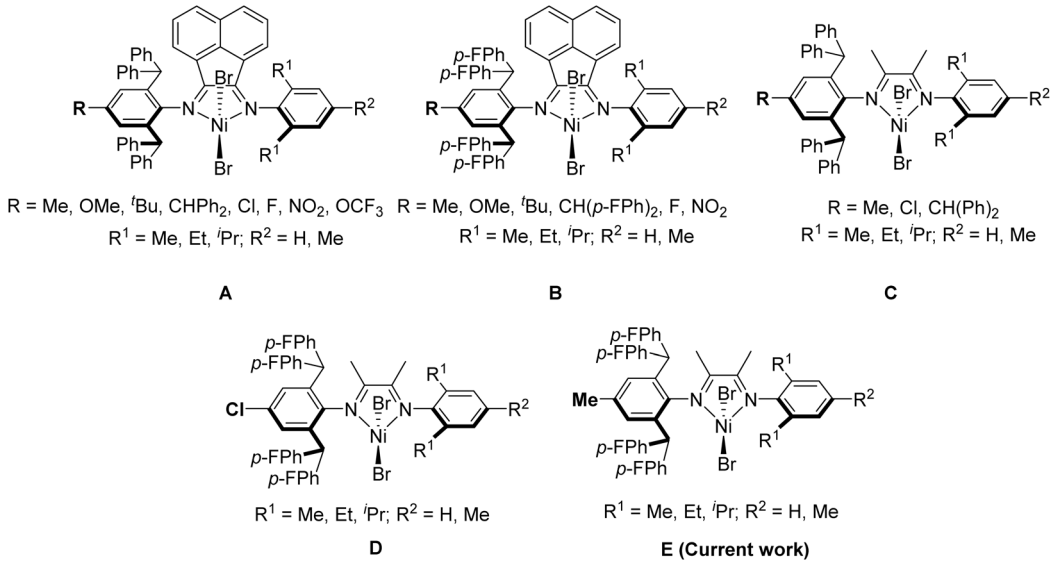

Scheme 1 Unsymmetrical bromonickel catalysts: 1,2-bis(arylimino)acenaphthenes (A–B) and 2,3-bis(arylimino)butane (C–E).

substituents with *N*-aryl moieties, especially eitherbenzhydryl ($CHPh_2$) or its fluorinated derivatives [$CH(p\text{-}FPh_2)$], guaranteeing higher activity and robust thermostability. For instance, the benzhydryl substituted $\mathbf{A_{CHPh2}}$ (ref. 37) and $\mathbf{C_{CHPh2}}$ (ref. 50) maintained high activity as 2.97×10^6 g(PE) mol^{-1} (Ni) h^{-1} at 90 °C and 1.70×10^6 g(PE) mol^{-1} (Ni) h^{-1} at 100 °C, respectively. Model **B** and **D** (Scheme 1), incorporating fluorobenzhydryl substituents, demonstrated higher activities and controlled the microstructures of resultant polyethylene elastomers (PEEs).[42–47,51] The remote fluorine has considered to effectively reduce the electron density around nickel centre in enhancing the ethylene coordination and boosting its catalytic activity.[46,52]

In general, nickel complexes incorporating electron-withdrawing groups ($\mathbf{A_F}$,[39] $\mathbf{B_F}$,[46] $\mathbf{C_{Cl}}$,[49] and **D**,[51] Scheme 1) demonstrated higher activity and yielded polyethylenes with higher molecular weights, their counterparts featuring electron-donating groups (especially in $\mathbf{A_{t\text{-}Bu}}$,[36] $\mathbf{B_{t\text{-}Bu}}$,[44] and $\mathbf{C_{Me}}$,[48] Scheme 1) produced polyethylenes with higher branching degrees (*e.g.*, $\mathbf{A_{Me}}$,[34] Scheme 1) and better mechanical properties ($\mathbf{A_{t\text{-}Bu}}$,[36] stress: 13.22 MPa, strain: 1002%, Scheme 1).

Additionally, the chlorinated precatalysts $\mathbf{C_{Cl}}$ (ref. 49) and **D** (ref. 51) (Scheme 1) generated bimodal polyethylenes characterized by a relative lower branching degree—a crucial factor closely associated with the inferior elastomeric properties observed in these branched polyethylenes. Contrastingly the polyethylene elastomer generated by *para*-methyl analogues ($\mathbf{A_{Me}}$,[34] $\mathbf{B_{Me}}$,[42] $\mathbf{C_{Me}}$,[48] Scheme 1) demonstrated unimodal and significantly higher branches.

Achieving the high-molecular-weight and high branched polyethylene elastomers by 2,3-bis(arylimino)butylnickel catalysts,[48,50,51] *para*-fluoro-benzhydryl substituents and *para*-methyl on the *N*-aryl moiety has been employed for the series of unsymmetrical 2,3-bis(arylimino)butylnickel complexes (**E**, Scheme 1). Interestingly, the new system performs high active and results unimodal and ultra-high molecular weights along with various branching degrees. The in-depth exploration, in turn, serves as a fundamental basis for the rational design and development of more efficient and precisely tuning α-diimine nickel precatalysts to prepare a wide range of high-value PEEs.

Results and discussion

Synthesis and characterization of ligands (L1–L5) and nickel complexes (Ni1–Ni5)

A straightforward two-step approach synthesis protocol was employed to prepare a series of 2-[2,6-bis(4,4′-difluorobenzhydryl)-4-methylphenylimino]-3-(2,6-R^1-4-R^2-phenyl) iminobutyl ligands (R^1 = Me, R^2 = H for **L1**; R^1 = Et, R^2 = H for **L2**; R^1 = ^{i}Pr, R^2 = H for **L3**; R^1 = R^2 = Me for **L4**; R^1 = Et, R^2 = Me for **L5**) (Scheme 2). Initially, the monoketone 3-[2,6-bis(4,4′-difluorobenzhydryl)-4-methylphenylimino]-2-butanone synthesized *via* a keto-amine condensation reaction between 2,3-

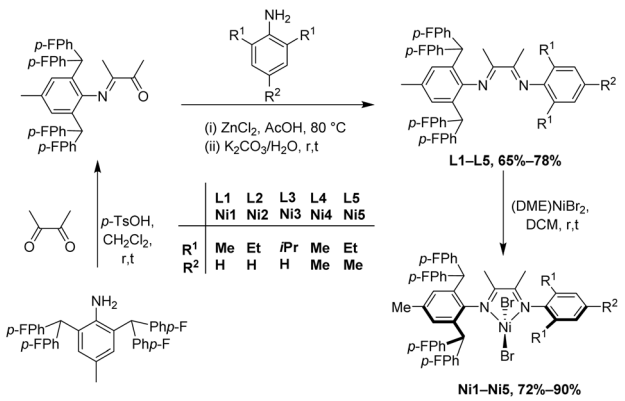

	L1	L2	L3	L4	L5
	Ni1	Ni2	Ni3	Ni4	Ni5
R^1	Me	Et	*i*Pr	Me	Et
R^2	H	H	H	Me	Me

Scheme 2 Synthesis route of ligands (L1–L5) and corresponding nickel complexes (Ni1–Ni5).

butanedione and 2,6-bis(4,4′-difluorobenzhydryl)-4-methylaniline, catalyzed by *p*-toluenesulfonic acid in dichloromethane (DCM) at room temperature, followed by recrystallization using methanol. Subsequently, the reaction of this monoketone with five anilines at 80 °C in acetic acid (99.5 w%) in the presence of zinc chloride ($ZnCl_2$) yielded zinc complexes as intermediates. The $ZnCl_2$ was then removed from the α-diimine zinc chloride intermediates by treatment with a saturated aqueous potassium carbonate solution (K_2CO_3) in DCM, resulting in the formation of the corresponding α-diimine ligands (**L1–L5**) with high yields (65–78%). The structures of all newly synthesized organic compounds were confirmed using $^1H/^{13}C$ NMR spectroscopy (Fig. S1–S12). Nickel bromide complexes were obtained with high yields (72–90%) by reacting the **L1–L5** ligands with $NiBr_2$(DME) in a 1.06 : 1 molar ratio in dichloromethane at ambient temperature (Scheme 2). FT-IR spectroscopy revealed imine functional groups with stretching frequencies ranging from 1636–1659 cm^{-1} in the ligands (Fig. S13), which shifted slightly to a lower range of 1636–1640 cm^{-1} in the corresponding nickel complexes (Fig. S14), indicating the occurrence of efficient coordination between the imine and nickel centers.[48] The purity and structural integrity of the organic compounds and nickel complexes were validated by carbon, hydrogen, and nitrogen elemental analysis.

Moreover, X-ray single crystal diffraction analysis of **Ni1** unveiled a tetra-coordinated structure, where the nickel atom is centrally positioned and coordinated by two nitrogen atoms from imine groups and two bromide atoms (Fig. 1). Notably, deviates from a regular tetrahedral geometry, aligning with previous reports on nickel complexes featuring the 2,3-bis(arylimino)butane ligand framework.[48,49,51] The phenyl rings in **Ni1**, derived from the *N*-2,6-bis(4,4′-difluorobenzhydryl)-4-methylphenyl and *N*-2,6-dimethylphenyl groups, are nearly perpendicular to the coordination plane defined by [C(2)–C(3)–N(2)–Ni(1)–N(1)], with angles of 90.0° and 85.8° in **Ni1**, respectively. These angles are significantly larger than those observed in analogs lacking the remote fluoro substituent (87.3° and 79.6° in $\mathbf{C_{Me}}$),[48] indicating that the introduction of remote fluoro group directly influences the open space around the nickel center, potentially impacting catalytic performance. Additionally, the Ni1–N2 bond lengths is slightly longer than the that of Ni1–N1 [2.012(7) Å *vs.* 2.009(8) Å], suggesting that the coordination of bulky *N*-aryl moiety with nickel center is slightly weaker compared to the smaller *N*-aryl unit, likely due to greater steric hindrance exhibited by the bulky *N*2-aryl moiety. Furthermore, it was observed that the bond angles N1–Ni1–N2 (81.0°) and Br1–Ni1–Br2 (119.24°) in **Ni1** are significantly smaller compared to those in the analogous acenaphthene-based complex $\mathbf{B_{Me}}$ (83.1° and 127.1°, respectively, Scheme 1)[42] indicating the diminished likelihood of chain-transfer reactions due to the crowded coordination environment could facilitate the synthesis of polyethylenes with higher molecular weights.[49]

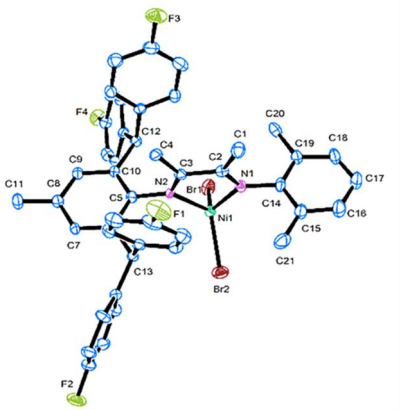

Fig. 1 ORTEP drawing of **Ni1**. Thermal ellipsoids are shown at the 30% probability level while the hydrogen atoms have been omitted for clarity. Selected bond lengths (Å): Ni(1)–N(1) 2.009(8), Ni(1)–N(2) 2.012(7), Ni(1)–Br(1) 2.3318(16), Ni(1)–Br(2) 2.3364(15), N(1)–C(2) 1.286(11), N(1)–C(14) 1.450(11), N(2)–C(3) 1.293(11), N(2)–C(5) 1.444(11) and bond angles (°): Br(1)–Ni(1)–Br(2) 119.24(6), N(1)–Ni(1)–Br(1) 118.9(2), N(1)–Ni(1)–Br(2) 106.5(2), N(1)–Ni(1)–N(2) 81.0(3), N(2)–Ni(1)–Br(1) 112.9(2), N(2)–Ni(1)–Br(2) 112.14(19).

Ethylene polymerization

Co-catalyst selection. In the quest to identify the optimal co-catalyst for ethylene polymerization, **Ni1** was systematically paired with a range of alkylaluminum reagents, namely methylaluminoxane (MAO), modified methylaluminoxane (MMAO), diethylaluminum chloride (Et_2AlCl), and ethylaluminum sesquichloride (EASC), to comprehensively evaluate its catalytic performance in ethylene polymerization under the specific conditions of 30 °C and a reaction duration of 30 minutes (entries 1–4, Table 1). The detailed result, presented in Table 1, revealed a hierarchy of catalytic activities for the different combinations: MAO (7.04×10^6 g(PE) mol^{-1} (Ni) h^{-1}) > MMAO (3.47×10^6 g(PE) mol^{-1} (Ni) h^{-1}) > Et_2AlCl (2.30×10^6 g(PE) mol^{-1} (Ni) h^{-1}) > EASC (0.33×10^6 g(PE) mol^{-1} (Ni) h^{-1}). Additionally, Et_2AlCl as a representative alkyl aluminum reagent was chosen to assess the performance of **Ni**/Et_2AlCl across varying temperature ranges, with the aim of elucidating its temperature-dependent behavior in ethylene polymerization.[48]

Catalytic evaluation of Ni/MAO system for ethylene polymerization. To optimize the polymerization conditions of the **Ni1**/MAO system and establish a reference standard for screening other nickel complexes, a systematic optimization study was conducted. The results presented in Table 2

Table 1 Ethylene polymerization for cocatalyst selection[a]

Entry	Co-catalyst	Al/Ni	Activity[b]	M_w[c]	M_w/M_n[c]	T_m[d]
1	MAO	2000	7.04	8.66	2.11	57.11
2	MMAO	2000	3.47	20.69	1.77	95.14
3	EASC	400	0.33	13.49	1.55	55.40
4	Et_2AlCl	600	4.27	9.02	3.37	41.18

[a] Conditions: 2 μmol **Ni1** and 100 mL toluene, 10 atm C_2H_4, 30 °C, 30 min. [b] 10^6 g(PE) mol^{-1} (Ni) h^{-1}. [c] M_w: 10^5 g mol^{-1}, M_w and M_w/M_n determined by GPC. [d] Determined by DSC.

Table 2 Catalytic evaluation using **Ni1**–**Ni5**/MAO for ethylene polymerization[a]

Entry	Precat.	T/°C	t/min	Al/Ni	Activity[b]	M_w[c]	M_w/M_n[c]	T_m[d]
1	**Ni1**	30	30	1000	2.17	11.51	3.51	107.41
2	**Ni1**	30	30	1500	4.20	8.12	2.04	95.31
3	**Ni1**	30	30	2000	7.04	8.66	2.11	57.11
4	**Ni1**	30	30	2500	6.61	6.91	2.01	56.57
5	**Ni1**	30	30	3000	6.50	4.33	1.53	48.31
6	**Ni1**	10	30	2000	0.80	14.95	2.06	110.10
7	**Ni1**	15	30	2000	5.80	22.34	1.59	120.77
8	**Ni1**	20	30	2000	9.84	12.33	1.85	88.82
9	**Ni1**	40	30	2000	5.11	7.47	2.35	37.87
10	**Ni1**	50	30	2000	4.70	7.30	2.67	33.96
11	**Ni1**	60	30	2000	3.19	6.12	2.25	21.08
12	**Ni1**	70	30	2000	1.94	4.33	1.52	—[g]
13	**Ni1**	20	5	2000	26.56	7.72	1.62	50.05
14	**Ni1**	20	15	2000	12.74	8.30	2.20	95.50
15	**Ni1**	20	45	2000	7.20	20.91	1.92	103.63
16	**Ni1**	20	60	2000	5.65	26.72	1.21	106.97
17[e]	**Ni1**	20	30	2000	3.58	8.33	3.97	81.55
18[f]	**Ni1**	20	30	2000	1.10	7.67	1.96	54.70
19	**Ni2**	20	30	2000	3.65	11.61	1.71	101.64
20	**Ni3**	20	30	2000	1.34	25.02	1.68	104.45
21	**Ni4**	20	30	2000	6.46	12.61	2.06	90.92
22	**Ni5**	20	30	2000	5.87	19.67	2.52	92.86

[a] Conditions: 2 μmol **Ni1** and 100 mL toluene, 10 atm C_2H_4. [b] 10^6 g(PE) mol^{-1} (Ni) h^{-1}. [c] M_w 10^5 g mol^{-1}, M_w and M_w/M_n determined by GPC. [d] Determined by DSC. [e] 5 atm of ethylene. [f] 1 atm of ethylene. [g] Broad and weak endotherms, amorphous-like polyethylenes.

unequivocally demonstrate that the catalytic activity of the **Ni1**/MAO system initially exhibited an upward trend as the Al/Ni molar ratio increased from 1000 : 1 to 2000 : 1, under the conditions of 30 °C and a 30-minute reaction time (entries 1–3, Table 2). A peak catalytic activity of 7.04 × 10^6 g PE mol^{-1} (Ni) h^{-1} was achieved at an Al/Ni ratio of 2000 : 1 (entry 3, Table 2). This phenomenon is likely attributed to the facilitated abstraction process of the halide ligand in the case of high co-catalyst dosage, which facilitates the formation of active species under these circumstances.[51] However, when the Al/Ni ratio was further increased to 3000 : 1, a decline in catalytic activity was observed, dropping to 6.50 × 10^6 g(PE) mol^{-1} (Ni) h^{-1} (entry 5, Table 2). This decrease can be explained by the fact that an excessive amount of MAO promotes chain transfer from the nickel active centers to the aluminum reagent. As a result, chain-termination reactions become more prevalent than chain-propagation reactions.[3] Notably, similar effects were also observed on the properties of the resulting polyethylenes. As the Al/Ni ratio increased from 1000 : 1 to 3000 : 1, the molecular weight of polyethylenes decreased from 11.51 × 10^5 to 4.33 × 10^5 g mol^{-1} (Fig. 2).[38,49] Simultaneously, the melting point dropped from 107.41 °C to 48.31 °C and the M_w/M_n narrowed from 3.51 to 1.53. These changes are all a consequence of the increased frequency of chain transfer to aluminum.

To thoroughly elucidate the temperature-dependent catalytic performance of the **Ni1**/MAO system, a series of experiments was conducted within 30-minute time-frame, spanning a temperature range from 10 °C to 70 °C (during

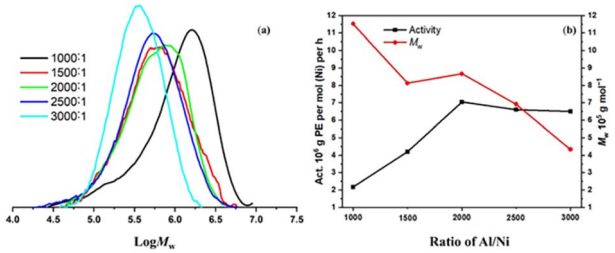

Fig. 2 (a) GPC traces and (b) plots of catalytic activity and M_w of the polyethylene produced using **Ni1**/MAO at different Al/Ni molar ratios (entries 1–5, Table 2).

polymerization, in the event of a temperature spike, cooling water was used to stabilize the temperature within ±3 °C of the set value within 1–2 minutes) while maintaining a fixed Al/Ni molar ratio of 2000 : 1 (entries 3, 6–12, Table 2). When the temperature was raised from 10 °C to 15 °C, a striking enhancement in catalytic activity was observed, with the activity surging from 0.80 × 10^6 to 5.80 × 10^6 g(PE) mol^{-1} (Ni) h^{-1} (entries 6 and 7, Table 2). This more than seven-fold increase strongly implies that at lower temperatures, the nickel centers were not fully activated, which hindered efficient initiation and chain propagation. The catalytic activity reached its peak at 20 °C, achieving an outstanding value of 9.84 × 10^6 g(PE) mol^{-1} (Ni) h^{-1} (entry 8, Table 2). However, as the temperature was further increased beyond 20 °C, a sharp decline in activity ensued, plummeting to 1.94 × 10^6 g(PE) mol^{-1} (Ni) h^{-1} at 70 °C. This decrease is likely due to the reduced solubility of ethylene in toluene and the decomposition of active species at higher temperatures.[46] Meanwhile, both the molecular weight and melting temperature of the polyethylenes generally decreased, with M_w dropping from 12.33 × 10^5 to 4.33 × 10^5 g mol^{-1} and T_m from 88.82 °C to a point where it was no longer detectable suggesting that at elevated temperatures, enhanced chain-transfer and chain-walking reactions occurred simultaneously. Notably, in contrast to the bimodal distribution of polyethylene produced by *para*-chloro substituted 2,3-bis(arylimino)butyl-nickel complexes **D** (Scheme 1),[51] all polyethylene obtained in current **Ni1**/MAO system exhibited unimodal distributions, confirming the retention of single-site catalytic characteristics (Fig. 3).

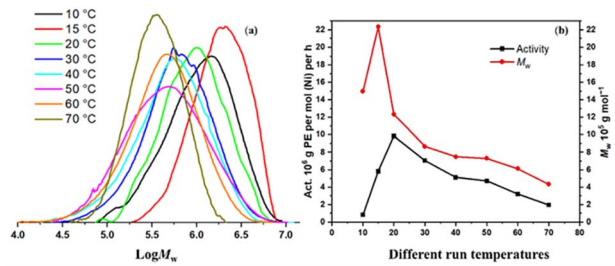

Fig. 3 (a) GPC traces and (b) plots of catalytic activity and M_w of the polyethylene produced using **Ni1**/MAO at different run temperatures (entries 8, 6–12, Table 2).

With the polymerization temperature fixed at 20 °C and the Al/Ni molar ratio at 2000 : 1, the polymerization time of the **Ni1**/MAO system was explored from 5 to 60 minutes (entries 8, 13–16, Table 2). At the outset, a 5-minute reaction duration unleashed an astonishing catalytic activity of 26.56×10^6 g(PE) mol^{-1} (Ni) h^{-1} indicating a rapid burst of activity fueled by the swift generation of active nickel species. As the reaction time was extended to 15, 45, and ultimately 60 minutes, a gradual decline in activity from 12.74×10^6 to 5.65×10^6 g(PE) mol^{-1} (Ni) h^{-1} occurred due to the progressive deactivation of active center.[36] Remarkably, even after 60 minutes, the current system retained a substantial level of activity, underscoring its significantly longevity. Meanwhile, the molecular weight of the resulting polyethylene steadily increased from 7.72×10^5 to 26.72×10^5 g mol^{-1} (Fig. 4), confirming the continuous growth of polymer chains over time.

A systematic investigation into the effects of ethylene pressure, which was varied from 1 to 10 atm, revealed a profound pressure-dependent modulation of both catalytic activity and the properties of the resulting polyethylenes. Catalytic activity exhibited a striking increase, rising from 1.10×10^6 g(PE) mol^{-1} (Ni) h^{-1} at 1 atm (entry 18, Table 2) to 3.58×10^6 g(PE) mol^{-1} (Ni) h^{-1} at 5 atm (entry 17, Table 2) and further to 9.84×10^6 g(PE) mol^{-1} (Ni) h^{-1} at 10 atm (entry 8, Table 2). This represents a three-fold and nine-fold enhancement under higher ethylene pressure, respectively (entries 8, 17 *vs.* entry 18, Table 2). This significant boost in activity could be attributed to the increasing concentration of ethylene molecules in the toluene under higher ethylene pressure, which effectively promotes the coordination and insertion process of ethylene.[44,47] Simultaneously, the molecular weight of the resulting polyethylenes followed an upward trend, escalating from 7.67×10^5 to 12.33×10^5 g mol^{-1} due to the suppression of chain-transfer reactions and the promotion of chain propagation under higher ethylene pressures. Additionally, the melting point value of the polyethylenes constantly increased from 54.70 °C to 88.82 °C, demonstrating a positive correlation with the applied ethylene pressure. This suggests that higher ethylene pressure could facilitate the formation of more ordered crystalline domains within the polymer matrix.

After establishing the most effective reaction conditions for **Ni1**/MAO system, the remaining four nickel pre-catalysts (**Ni2**–**Ni5**) were evaluated under similar condition to discern the influence of ligand framework on catalytic performance (entries 8, 19–22, Table 2). All nickel catalysts demonstrated commendable activity, with values ranging from 1.34×10^6 to 9.84×10^6 g(PE) mol^{-1} (Ni) h^{-1}. Additionally, varying the *N*-aryl moiety of the nickel complexes was found to fine-tune the activity and polyethylene properties.[37,46] Specifically, the activity order was **Ni1** [2,6-di(Me)] > **Ni4** [2,4,6-tri(Me)] > **Ni2** [2,6-di(Et)] > **Ni5** [2,6-di(Et)-4-Me]> **Ni3** [2,6-di(^{i}Pr)], revealing that bulkier *ortho*-substituents could impede the coordination/insertion of ethylene, thereby reducing the polymerization activity. Conversely, the M_w of the resulting polyethylene followed a different order: **Ni3** [2,6-di(^{i}Pr)] > **Ni5** [2,6-di(Et)-4-Me] > **Ni4** [2,4,6-tri(Me)] > **Ni1** [2,6-di(Me)] > **Ni2** [2,6-di(Et)] (Fig. 5) reflecting that the introduction of bulky *ortho*-substituent and *para*-methyl substituents is beneficial for protecting or stabilizing the active nickel center, thereby suppressing chain transfer reactions and enabling the formation of longer polymer chains. Consequently, **Ni3**, which contains the bulkiest *ortho*-isopropyl group, showed the lowest activity but produced polyethylenes with the highest molecular weight.

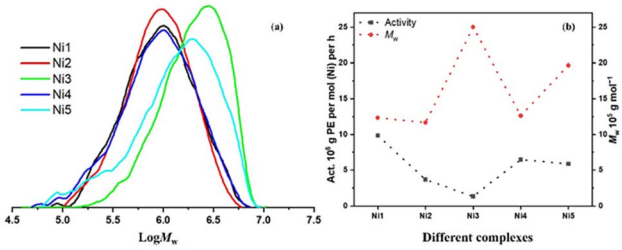

Fig. 5 (a) GPC traces and (b) plots of the catalytic activity and M_w of the polyethylene produced using **Ni1**–**Ni5** on activation with MAO (entries 8, 19–22, Table 2).

Catalytic evaluation of Ni/Et$_2$AlCl system for ethylene polymerization. Temperature and co-catalyst type are pivotal factors that exert a profound influence on the regulation of polyethylene microstructures. Consequently, the secondary active co-catalyst Et$_2$AlCl was selected to assess its performance across a range of temperatures (entries 1–7, Table 3). As illustrated in Fig. 6, a marked decrease in the values of catalytic activity,

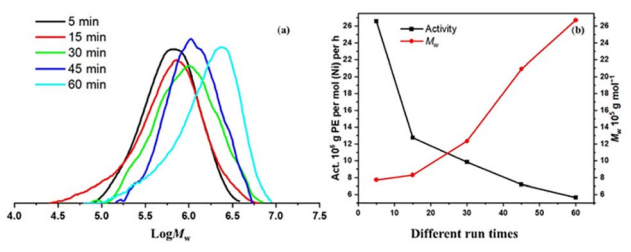

Fig. 4 (a) GPC traces and (b) plots of catalytic activity and M_w of the polyethylene produced using **Ni1**/MAO at different run times (entries 8, 13–16, Table 2).

Table 3 Catalytic evaluation at different temperatures using **Ni1**/Et$_2$AlCl for ethylene polymerization[a]

Entry	*T*/°C	Activity[b]	M_w[c]	M_w/M_n[c]	T_m[d]
1	20	4.67	10.90	6.81	55.40
2	30	4.27	9.02	3.38	41.18
3	40	4.07	6.57	2.29	39.62
4	50	3.82	5.29	2.19	15.94
5	70	3.20	5.15	1.72	—[e]
6	80	2.92	4.64	2.23	—[e]
7	90	2.56	2.67	1.21	—[e]

[a] Conditions: 2 μmol **Ni1** and 100 mL toluene, 10 atm C_2H_4, 30 min, Al/Ni = 600. [b] 10^6 g(PE) mol^{-1} (Ni) h^{-1}. [c] M_w: 10^5 g mol^{-1}, M_w and M_w/M_n determined by GPC. [d] Determined by DSC. [e] Broad and weak endotherms, amorphous-like polyethylenes.

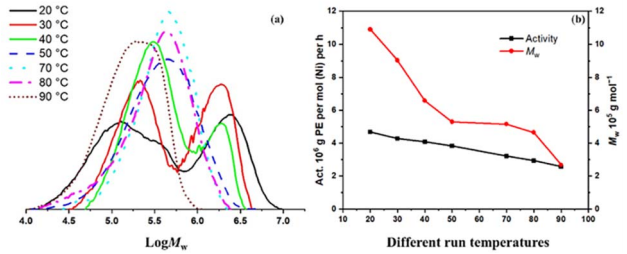

Fig. 6 (a) GPC traces and (b) plots of catalytic activity and M_w of the polyethylene produced using **Ni1**/Et_2AlCl at different run temperatures (Table 3).

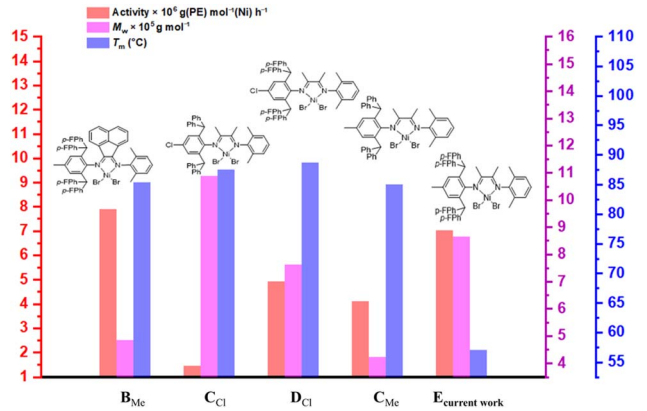

Fig. 7 A comparative analysis of the catalytic performance among a series of α-diimine nickel complexes, featuring either the 1,2-bis(arylimino)acenaphthene or the 2,3-bis(arylimino)butane ligand backbone, was conducted under identical polymerization conditions (Al/Ni ratios of 2000 : 1, 30 °C, 30 min, 10 atm).

molecular weight (M_w), and melting temperature (T_m) as the temperature increased (entries 3, 6–12, Table 2). The polyethylenes synthesized at lower temperatures (20–40 °C) displayed bimodal characteristics, which were distinct from those obtained in **Ni1**/MAO system. This disparity is likely attributable to the distinct alkylation behaviors of MAO and Et_2AlCl. MAO, with its steric hindrance, facilitates the formation of single-site active species through a more accessible orientation. In contrast, Et_2AlCl allows for the generation of cationic active species with diverse conformations due to the flexibility of the C2–C3 bond.[49] Conversely elevating temperatures (50–90 °C),[50] the polyethylenes exhibited a unimodal and narrow molecular weight distribution implying that the increased thermal energy prompts the catalyst active centers to become more homogeneous, resulting in a narrower molecular weight distribution. Notably, when comparing high-temperature experiments, the decline in activity of the **Ni1**/Et_2AlCl system (2.67×10^6 g(PE) mol^{-1} (Ni) h^{-1} at 90 °C) was significantly lower than that of the **Ni1**/MAO system (1.94×10^6 g(PE) mol^{-1} (Ni) h^{-1} at 70 °C), indicating the superior thermal stability of the former system.

Catalytic comparison with previous reports. For the sake of comparison, the catalytic activities and molecular weights (M_w) of polyethylenes synthesized by a series of previously reported and newly prepared nickel complexes bearing the *N*-2,6-dimethylphenyl, **B–E**, under same polymerization conditions are presented in Fig. 7. The bar chart unequivocally illustrates that, under identical polymerization conditions, the catalytic activities of these nickel complexes follow the sequence: $\mathbf{B_{Me}}$ (ref. 42) > **E** (current work) > $\mathbf{D_{Cl}}$ (ref. 51) > $\mathbf{C_{Me}}$ (ref. 48) > $\mathbf{C_{Cl}}$ (ref. 49). Conversely, the M_w values of the resulting polyethylenes exhibit a distinct pattern: $\mathbf{C_{Cl}}$ (ref. 49) > **E** > $\mathbf{D_{Cl}}$ (ref. 51) > $\mathbf{B_{Me}}$ (ref. 42) > $\mathbf{C_{Me}}$.[48] This trend suggests that the two *para*-methyl substituted nickel complexes ($\mathbf{B_{Me}}$ and **E**) demonstrate superior activity within this series, attributable to the enhanced solubility of the nickel complexes in toluene implying that the incorporation of an *ortho*-difluorobenzhydryl group along with a *para*-methyl group synergistically enhances catalytic activity. In contrast, complex **E** yielded significantly higher molecular weight values compared to $\mathbf{B_{Me}}$, underscoring the profound influence of the ligand backbone on the coordination environment. This, in turn, affects the coordination/insertion of ethylene and the chain transfer process during polymerization. In addition, when compared to the *para*-methyl substituted $\mathbf{C_{Me}}$ complex, the *para*-chloro substituted $\mathbf{C_{Cl}}$ complexes produced polyethylene with a relatively higher molecular weight and melting point. This is likely attributable to the electron-withdrawing effect of the chloro group, which increases the molecular weight and reduces branching degree of the resulting polyethylenes.[3] However, when remote fluoro groups were introduced into the benzhydryl moiety of the $\mathbf{C_{Cl}}$ complex, the resulting $\mathbf{D_{Cl}}$ complex yielded polyethylenes with a significantly lower molecular weight, demonstrating that an excessive electron-withdrawing influence exerted on the nickel center can destabilize the active catalytic site, thereby reducing the molecular weight of polyethylenes produced. In contrast, the combination of an *ortho*-difluorobenzhydryl group and a *para*-methyl substituent (**E**) led to a substantial increase in the molecular weight of the polyethylenes, albeit at the expense of a significantly reduced melting point. This phenomenon is presumably due to the moderate electron-withdrawing effect provided by the remote fluoro groups, which is beneficial for stabilizing the nickel active species during polymerization.[3] Moreover, the polyethylene synthesized by catalyst **E** (Scheme 1) displayed the lowest melting temperature, approximately 57.11 °C, accompanied by a broad peak indicative of its amorphous state. This amorphous nature arises from the high degree of branching introduced by the chain-walking mechanism.[36] To summarize, the catalyst **E** proposed in the current study achieves a favorable balance of excellent catalytic activity, a reasonable molecular weight, and high branching. This combination is advantageous for optimizing the mechanical properties of polyethylenes and opens up new avenues for their application.

Microstructure of the polyethylenes. To systematically evaluate the branching architecture of polyethylenes, five representative samples namely PE-MAO-20, PE-MAO-30, and PE-MAO-70 (entries 8, 3, and 12 in Table 2) and PE-Et_2AlCl-20 and PE-Et_2AlCl-70 (entries 2 and 5 in Table 3), were prepared using the **Ni1**/MAO and **Ni1**/Et_2AlCl systems and subsequently subjected to high-temperature ^{13}C NMR spectroscopic analysis.

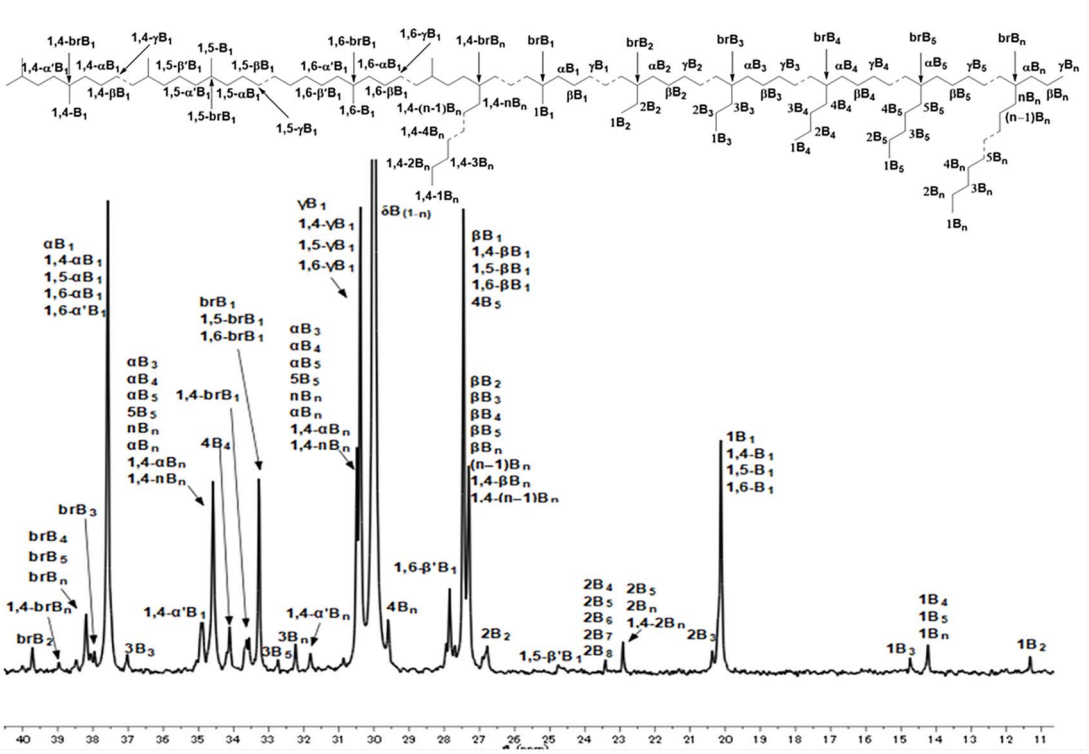

Fig. 8 High temperature ^{13}C NMR spectrum of PE-MAO-50 sample (entry 10, Table 2).

The high-temperature ^{13}C NMR spectra were acquired in deuterated 1,1,2,2-tetrachloroethane-d_2 at 110 °C, and the resulting spectral data are depicted in Fig. 8 and S15–S18. By utilizing established literature-based assignments, the branching content and types within the polyethylene samples were precisely determined and analyzed.[53] A distinct temperature-dependent trend was observed in both **Ni1**/MAO (62–200/1000 C) and **Ni1**/Et_2AlCl (126–201/1000 C) system. Elevated polymerization temperatures facilitated the formation of polyethylenes with a higher degree of branching, owing to the increased likelihood of chain walking. Concurrently, in the **Ni1**/MAO system, an increase in the branching degree from 126/1000 C to 201/1000 C (Table 4) resulted in a significant reduction in the melting temperature (T_m) from 88.82 °C to a point where it was no longer detectable. This was accompanied by a concurrent decline in crystallinity from 57.91% to a fully amorphous state.[48] Notably, the PE-MAO-70 sample exhibited a significantly high branching degree up to 200/1000 C highlighting that the **Ni1**/MAO system exhibited unique catalytic behavior under elevated temperatures (entry 12, Table 2). A comparative analysis of polyethylenes synthesized *via* the **Ni1**/MAO and **Ni1**/Et_2AlCl systems further unveils distinct trends with PE-Et_2AlCl-20 sample exhibiting a higher branching degree, a lower melting temperature and reduced crystallinity compared to the PE-MAO-20 sample (126/1000 C, 55.40 °C, 32.50% *vs.* 62/1000 C, 88.82 °C, 57.91%, respectively). However, when subjected to a high polymerization temperature of 70 °C, the PE-Et_2AlCl-70 and PE-MAO-70 samples demonstrate comparable branching degree (approximately 200/1000 C) and a similar amorphous state. The varying microstructures of the polyethylenes, resulting from different polymerization conditions, ultimately exert a significant influence on their

Table 4 Branching analysis of the PE samples obtained using **Ni1**/MAO and **Ni1**/Et_2AlCl at different temperatures

		Branching composition (%)							
PE sample	Branches/1000C	Me	Et	Pr	Bu	Amyl	Longer branch	T_m[a] (°C)	X_c[a] (%)
PE-MAO-20	62	77.7	2.9	2.1	8.8	1.9	6.6	88.82	57.91
PE-MAO-50	133	79.3	4.4	4.1	6.3	2.3	3.6	33.96	13.68
PE-MAO-70	200	78.3	1.8	4.5	5.7	2.6	7.0	—	—
PE-Et_2AlCl-20	126	72.4	3.3	5.0	7.0	8.0	4.3	55.44	32.50
PE-Et_2AlCl-70	201	75.3	4.2	3.9	8.6	2.6	5.4	—	—

[a] Determined by DSC; $X_c = \Delta H_f(T_m) = \Delta H_f^{\circ}(T_m^{\circ})$; $\Delta H_f^{\circ}(T_m^{\circ}) = 248.3$ J g^{-1}.

Table 5 Selected properties of the PE samples obtained using **Ni1** by MAO/Et_2AlCl with various run temperatures

PE sample	T (°C)	M_w[a]	T_m[b]	X_c[b] (%)	σ_b[c] (MPa)	ε_b[c] (%)	SR[d] (%)
PE-MAO-20	20	12.33	88.82	57.91	13.42	388	40
PE-MAO-50	50	7.30	33.96	13.68	5.48	431	73
PE-MAO-70	70	4.33	—[e]	—[e]	1.68	529	21
PE-Et_2AlCl-20	20	10.90	55.40	32.50	3.77	239	59
PE-Et_2AlCl-50	50	5.29	15.94	6.56	1.46	177	65
PE-Et_2AlCl-70	70	5.19	—[e]	—[e]	1.03	267	42

[a] Determined by GPC, values $\times 10^5$ g mol^{-1}. [b] Determined by DSC; $X_c = \Delta H_f(T_m) = \Delta H_f^{\circ}(T_m^{\circ})$; $\Delta H_f^{\circ}(T_m^{\circ}) = 248.3$ J g^{-1}. [c] Determined by using a universal tester. [d] Strain recovery values (SR) were calculated by using the standard formula SR $= 100(\varepsilon_a - \varepsilon_r)/\varepsilon_a$, where ε_a is the applied strain and ε_r is the strain in the cycle at 0 loads after 10 cycles. [e] Broad and weak endotherms, amorphous-like polyethylenes.

mechanical properties, a topic that will be explored in subsequent sections.

Mechanical properties of the polyethylenes. To evaluate the mechanical properties of the branched polyethylenes synthesized, six samples were selected, generated using **Ni1**/MAO and **Ni1**/Et_2AlCl systems at varying reaction temperatures (20 °C, 50 °C and 70 °C). Each sample underwent both a tensile stress–strain test using a universal testing machine and a stress–strain recovery test *via* dynamic mechanical analysis (DMA). The comprehensive results are presented in Table 5. Initially, monotonic tensile stress–strain measurements were conducted at room temperature, with each test involving three specimens to ensure data consistency. The stress–strain curves are depicted in Fig. 9a and 10a. The molecular weight and branching degree of polyethylenes were closely linked to their mechanical properties.[36,37] Specifically, PE-MAO-20 exhibits a relatively low branching degree (62/1000 C), high molecular weight (12.33 $\times$ 10^5 g mol^{-1}) and high crystallinity (57.91%), resulting in high tensile strength (σ_b = 13.42 MPa) and high elongation at break (ε_b = 388%). As the temperature increased to 50 °C and 70 °C, the branching degree rose from 133/1000 C to 200/1000 C, disrupting the regular packing of polymer chains and sharply reducing melting temperature and crystallinity. Consequently, the strength of polyethylenes decreases from 5.48 MPa to 1.68 MPa.[48] As the crystallinity of polyethylenes decreases from 13.68% to approach an amorphous-like state, the elongation at break increases from 431% to 529% (Table 5) indicating that the amorphous regions can undergo molecular chain slippage and rearrangement when subjected to stress, thereby absorbing more energy and exhibiting higher toughness. For the **Ni1**/Et_2-AlCl-based samples, PE-Et_2AlCl-20 showed lower initial tensile strength (3.77 MPa *vs.* 13.43 MPa) and elongation (239% *vs.* 388%) compared to PE-MAO-20, consistent with its lower molecular weight (10.90 $\times$ 10^5 g mol^{-1} *vs.* 12.33 $\times$ 10^5 g mol^{-1}) and lower crystallinity (32.50% *vs.* 57.91%). Further increasing the temperature led to a continuous reduction in mechanical properties (Fig. 10a), with PE-Et_2AlCl-70 having the lowest tensile strength (1.03 MPa).

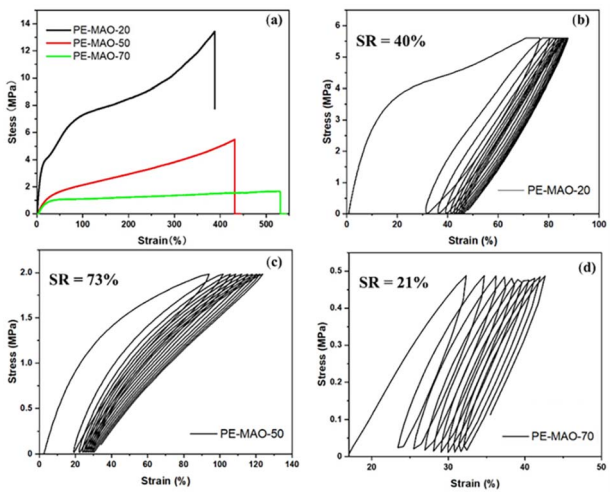

Fig. 9 (a) Stress–strain curves and (b–d) recovery tests for the selected polyethylene samples, PE-MAO-20, PE-MAO-50, and PE-MAO-70.

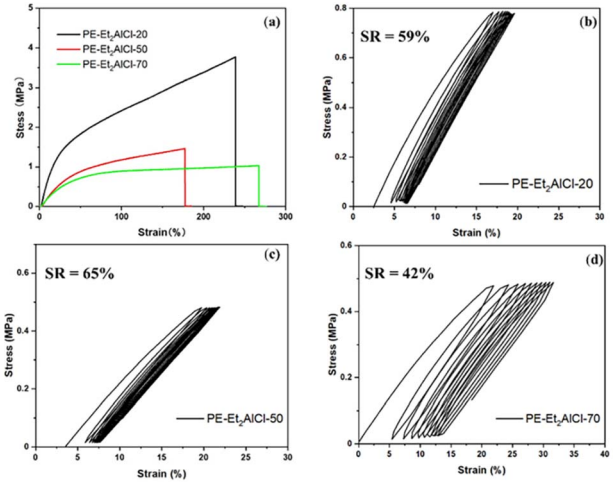

Fig. 10 (a) Stress–strain curves and (b–d) recovery tests for the selected polyethylene samples, PE-Et_2AlCl-20, PE-Et_2AlCl-50, and PE-Et_2AlCl-70.

To further investigate the elastomeric properties of these polyethylenes, stress–strain recovery tests were conducted using dynamic mechanical analysis (DMA), and the results are presented in Fig. 9b–d and 10b–d. These tests were typically performed at 30 °C, with each cycle being repeated up to 10 times. After the first cycle, the stress–strain hysteresis loops of all samples exhibited consistent recovery levels indicating that all the polyethylenes display the characteristics of polyethylene elastomers.[41] Based on the DSC and high temperature ^{13}C NMR results presented earlier, it is evident that as the temperature increased, the polyethylenes with different branching degrees transition from a semi-crystalline state to a fully amorphous state. Consequently, PE-MAO-20, with high crystallinity (X_c = 57.91%), exhibited a limited stress–strain recovery value of merely 40% due to its relatively low branching degree (62/1000 C) and insufficient soft segments. In contrast, PE-MAO-70 with

an extremely high branching degree (200/1000 C), becomes a fully amorphous and soft material with fewer hard segments, exhibiting a low stress–strain recovery value of 21%.[48] For the sample PE-MAO-50, which had a moderate branching degree (133/1000 C) and crystallinity (13.68%), a balance between hard and soft segments is achieved, resulting in the highest stress–strain recovery value of up to 73%, a value comparable to those obtained by previously reported unsymmetrical α-diimine nickel precatalysts.[48] Similarly, comparable stress–strain recovery values were observed for the **Ni1**/Et_2AlCl system (SR for PE-Et_2AlCl-20, 59%; SR for PE-Et_2AlCl-50, 65%; SR for PE-Et_2-AlCl-70, 42%, Table 5). In summary, an ideal branching degree and sufficient crystallinity are essential for obtaining optimal elastomeric properties, as these factors facilitate the formation of balanced hard and soft regions.

Conclusions

In this study, a series of unsymmetrical 2-[2,6-bis(4,4′-difluorobenzhydryl)-4-methylphenylimino]-3-arylimino-butylnickel precatalysts has been successfully synthesized and comprehensively characterized. These nickel precatalysts demonstrated remarkable catalytic performance during ethylene polymerization, characterized by high activity, excellent thermal stability, and the ability to tailor the properties of the resulting polyethylenes. Notably, the current system maintained a high level of catalytic activity at high temperature, which reached up to 1.94×10^6 g(PE) mol^{-1} (Ni) h^{-1} at 70 °C in **Ni**/MAO system and 2.56×10^6 g(PE) mol^{-1} (Ni) h^{-1} even at 90 °C in **Ni**/Et_2AlCl system. Furthermore, the polymerization temperature emerged as a crucial factor influencing the microstructure and physical properties of the produced polyethylenes. As the reaction temperature rose, there was a significant increase in the branching degree, ranging from 62 to 201 branches/1000 C. Concurrently, the crystallinity decreased, transitioning the polyethylenes from a semi-crystalline state to a completely amorphous state. The synergistic interplay among molecular weight, controlled branching degree, and crystallinity, which struck a balance between hard and soft segments, enabled the polyethylene synthesized in this work to exhibit both high mechanical strength (up to 13.42 MPa) and an elastic recovery of 73%. Consequently, it shows great promise as a material for advanced polyethylene elastomer applications.

Experimental

Synthesis of monoketone and ligands (L1–L5)

3-[2,6-Bis(4,4′-difluorobenzhydryl)-4-methylphenylimino]-2-butanone. In a 300 mL solution of dichloromethane (DCM), a mixture was prepared by combining 2,6-bis(4,4′-difluorobenzhydryl)-4-methylaniline (10.24 g, 20.0 mmol), 2,3-butanedione (1.72 g, 20.0 mmol), and a catalytic amount of *p*-toluenesulfonic acid (0.57 g, 3.0 mmol). The resulting mixture was vigorously stirred at room temperature for a duration of 4 hours. Subsequently, the solvent was removed under reduced pressure through evaporation. The crude product obtained was then subjected to purification by recrystallization from methanol.[54] This purification process yielded a bright yellow solid (8.82 g, 76%). ^{1}H NMR (400 MHz, $CDCl_3$, TMS): δ 6.69–6.94 (m, 16H, Ar–H), 6.60 (s, 2H, Ar–H), 5.06 (s, 2H, Ar–CH$(Ph)_2$), 2.30 (s, 3H, O=C–CH_3), 2.17 (s, 3H, Ar–CH_3), 0.86 (s, 3H, N=C–CH_3). ^{13}C NMR (100 MHz, $CDCl_3$, TMS): δ 199.3 (O=*C*–CH_3), 168.8 (N=*C*–CH_3), 162.8, 160.4, 144.3, 138.7, 138.3, 137.9, 131.1, 131.0, 130.8, 130.7, 128.9, 115.8, 115.7, 115.3, 115.1, 50.8, 25.0, 21.4, 14.9. FT-IR (cm^{-1}): 2956 (w), 2902 (w), 2854 (w), 1702 (s, $\nu_{C=O}$), 1653 (m), 1602 (w), 1504 (s), 1455 (m), 1417 (m), 1353 (m), 1157 (s), 1115 (m), 1096 (m), 1015 (m), 867 (w), 834 (s), 768 (m), 733 (m), 710 (w), 662 (w). Anal. calcd for $C_{37}H_{29}F_4NO$ (579.64): C,76.67; H, 5.04; N, 2.42%. Found; C, 76.75; H, 5.39; N, 2.63%.

2-[2,6-Bis(4,4′-difluorobenzhydryl)-4-methylphenylimino]-3-(2,6-R^1-4-R^2-phenyl)imino-butyl ligands (L1–L5)

L1, R^1 = Me, R^2 = H. A 25 mL round-bottom flask, equipped with a magnetic stir bar, was charged with zinc(II) chloride (0.50 g, 1.5 mmol), 2,6-dimethylaniline (0.18 g, 1.5 mmol), 3-[2,6-bis(4,4′-difluorobenzhydryl)-4-methylphenylimino]-2-butanone (0.87 g, 1.5 mmol), and 1 mL of acetic acid. The reaction mixture was then heated to 80 °C and stirred magnetically for 4 hours. After cooling the mixture to room temperature, 10 mL of diethyl ether was added. This addition led to the formation of a yellow precipitate (zinc(II) chloride complex), which was subsequently isolated by filtration. The intermediate zinc(II) chloride complex was dissolved in dichloromethane (50 mL). A saturated aqueous solution of potassium carbonate was then added to the DCM solution and the resulting mixture was stirred at room temperature for 1.5 hours.[55–57] The organic layer was separated using a separatory funnel, washed three times with deionized water and then dried over anhydrous magnesium sulfate. After removing the solvent by rotary evaporation, the crude product was recrystallized from *n*-hexane, yielding **L1** as a bright yellow powder (0.80 g, 78%). ^{1}H NMR (400 MHz, $CDCl_3$, TMS): δ 7.06–7.01 (m, 6H, Ar–H), 6.97–6.91 (m, 13H, Ar–H), 6.60 (s, 2H, Ar–H), 5.18 (s, 2H, Ar–CH(*p*-FPh)$_2$), 2.18 (s, 3H, Ar–CH_3), 1.98 (s, 6H, Ar–CH_3), 1.79 (s, 3H, N=C–CH_3), 1.01 (s, 3H, N=C–CH_3). ^{13}C NMR (100 MHz, $CDCl_3$, TMS): δ 170.0 (N=*C*–CH_3), 167.5 (N=*C*–CH_3),162.8, 162.8, 160.4, 160.3, 145.5, 139.1, 138.2, 132.4, 131.5, 131.1, 130.9, 128.8, 128.1, 124.4, 123.5, 115.7, 115.5, 115.2, 115.0, 50.9, 21.4, 18.0, 16.4, 15.9. FT-IR (cm^{-1}): 2919 (w), 2885 (w), 1645 (m, $\nu_{C=N}$), 1601 (m), 1478 (s), 1474 (m), 1449 (w), 1415 (w), 1361 (m), 1304 (w), 1215 (s), 1205 (s), 1201 (w), 1156 (m), 1121 (m), 1095 (m), 1042 (w), 1014 (w), 937 (w), 875 (w), 832 (s), 795 (m), 767 (m), 733 (m), 688 (w), 656 (w). Anal. calcd for $C_{45}H_{38}F_4N_2$ (682.81): C, 79.16; H, 5.61; N, 4.10%. Found; C, 79.33; H, 5.82; N, 4.56%.

L2, R^1 = Et, R^2 = H. Adopting a synthetic strategy akin to that utilized for the synthesis of **L1**, the substitution of 2,6-dimethylaniline with 2,6-diethylaniline led to the formation of **L2** as a yellow solid (0.78 g, 73%). ^{1}H NMR (400 MHz, $CDCl_3$, TMS): δ 7.11–7.09 (d, J = 8.0 Hz, 2H, Ar–H), 7.06–7.02 (m, 5H, Ar–H), 6.99–6.93 (m, 12H, Ar–H), 6.61 (s, 2H, Ar–H), 5.20 (s, 2H, Ar–CH(*p*-FPh)$_2$), 2.34–2.23 (m, 4H, Ar–CH_2CH_3), 2.19 (s, 3H, Ar–

CH_3), 1.82 (s, 3H, N=C–CH_3), 1.17 (s, J = 8.0 Hz, 6H, Py–CH_2CH_3), 1.03 (s, 3H, N=C–CH_3). ^{13}C NMR (100 MHz, $CDCl_3$, TMS): δ 170.0 (N=C–CH_3), 167.5 (N=C–CH_3), 162.9, 162.8, 160.4, 160.3, 147.3, 145.5, 139.2, 138.2, 132.4, 131.4, 131.2, 130.9, 130.8, 130.6, 130.2, 128.9, 126.1, 123.4, 115.7, 115.5, 115.3, 115.0, 50.9, 24.6, 21.4, 16.4, 13.8. FT-IR (cm^{-1}): 2965 (w), 2929 (w), 2901 (w), 1643 (m, $\nu_{C=N}$), 1601 (m), 1458 (s), 1448 (m), 1413 (w), 1360 (m), 1299 (w), 1222 (s), 1198 (w), 1097 (m), 1014 (m), 965 (w), 933 (w), 874 (w), 831 (s), 798 (m), 759 (w), 734 (m), 685 (w), 656 (w). Anal. calcd for $C_{47}H_{42}F_4N_2$ (710.86): C,79.41; H, 5.96; N, 3.94%. Found; C, 79.10; H, 5.68; N, 4.31%.

L3, R^1 = ^{i}Pr, R^2 = H. Adopting a synthetic strategy akin to that utilized for the synthesis of **L1**, the substitution of 2,6-dimethylaniline with 2,6-diisopropylaniline led to the formation of **L3** as a yellow solid (0.78 g, 73%). ^{1}H NMR (400 MHz, $CDCl_3$, TMS): δ 7.16–6.95 (m, 19H, Ar–H), 6.60 (s, 2H, Ar–H), 5.19 (s, 2H, Ar–CH(p-FPh)$_2$), 2.59–2.52 (m, 2H, Ar–CH(CH_3)$_2$), 2.18 (s, 3H, Ar–CH_3), 1.47 (s, 3H, N=C–CH_3), 1.22 (d, J = 8.0 Hz, 6H, Ar–CH(CH_3)$_2$), 1.17 (d, J = 8.0 Hz, 6H, Ar–CH(CH_3)$_2$), 1.01 (s, 3H, N=C–CH_3). ^{13}C NMR (100 MHz, $CDCl_3$, TMS): δ 170.1 (N=C–CH_3), 167.7 (N=C–CH_3), 162.9, 162.8, 160.4, 160.3, 146.0, 145.5, 139.2, 138.2, 134.9, 132.4, 131.4, 131.1, 131.0, 130.9, 130.8, 128.9, 124.1, 123.2, 115.7, 115.5, 115.3, 115.0, 50.9, 28.4, 23.4, 23.2, 21.4, 16.7, 16.5. FT-IR (cm^{-1}): 2962 (w), 2919 (w), 2900 (w), 1639 (m, $\nu_{C=N}$), 1602 (m), 1480 (s), 1460 (w), 1434 (w), 1359 (m), 1325 (m), 1304 (w), 1221 (s), 1190 (w), 1157 (m), 1098 (m), 1047 (w), 1015 (m), 957 (w), 935 (w), 876 (w), 832 (s), 785 (m), 764 (m), 736 (w), 688 (w), 656 (w). Anal. calcd for $C_{49}H_{46}F_4N_2$ (738.91): C, 79.65; H, 6.28; N, 3.79%. Found; C, 80.01; H, 6.60; N, 3.29%.

L4, R^1 = Me, R^2 = Me. Adopting a synthetic strategy akin to that utilized for the synthesis of **L1**, the substitution of 2,6-dimethylaniline with 2,4,6-trimethylaniline led to the formation of **L4** as a yellow solid (0.75 g, 72%). ^{1}H NMR (400 MHz, $CDCl_3$, TMS): δ 7.05–6.88 (m, 18H, Ar–H), 6.61 (s, 2H, Ar–H), 5.19 (s, 2H, Ar–CH(p-FPh)$_2$), 2.29 (s, 3H, Ar–CH_3), 2.19 (s, 3H, Ar–CH_3), 1.95 (s, 6H, Ar–CH_3), 1.80 (s, 3H, N=C–CH_3), 1.01 (s, 3H, N=C–CH_3). ^{13}C NMR (100 MHz, $CDCl_3$, TMS): δ 170.1 (N=*C*–CH_3), 167.7 (N=*C*–CH_3), 162.9, 162.8, 160.4, 160.3, 145.9, 145.5, 139.1, 138.2, 138.1, 132.7, 132.3, 131.5, 131.2, 130.9, 130.8, 128.9, 128.8, 50.9, 21.4, 20.8, 18.0, 16.4, 15.8. FT-IR (cm^{-1}): 2919 (w), 2909 (w), 2890 (w), 1659 (m, $\nu_{C=N}$), 1635 (m), 1602 (m), 1501 (s), 1474 (m), 1455 (m), 1421 (w), 1361 (m), 1302 (w), 1220 (s), 1158 (s), 1125 (m), 1099 (m), 1044 (w), 1013 (m), 964 (w), 933 (w), 832 (s), 799 (m), 723 (m), 679 (w). Anal. calcd for $C_{46}H_{40}F_4N_2$ (696.83): C, 79.29; H, 5.79; N, 4.02%. Found; C, 78.89; H, 6.08; N, 4.32%.

L5, R^1 = Et, R^2 = Me. Adopting a synthetic strategy akin to that utilized for the synthesis of **L1**, the substitution of 2,6-dimethylaniline with 2,6-diethyl-4-methylaniline led to the formation of **L5** as a yellow solid (0.79 g, 73%). ^{1}H NMR (400 MHz, $CDCl_3$, TMS): δ 7.05–6.91 (m, 18H, Ar–H), 6.61 (s, 2H, Ar–H), 5.20 (s, 2H, Ar–CH(p-FPh)$_2$), 2.32 (s, 3H, Ar–CH_3), 2.26–2.23 (m, 4H, Ar–CH_2CH_3), 2.19 (s, 3H, Ar–CH_3), 1.82 (s, 3H, N=C–CH_3), 1.16 (t, J = 4 Hz, 6H, Py–CH_2CH_3), 1.02 (s, 3H, N=C–CH_3). ^{13}C NMR (100 MHz, $CDCl_3$, TMS): δ 170.1 (N=C–CH_3), 167.7 (N=C–CH_3), 162.9, 162.8, 160.4, 160.3, 145.5, 144.9, 139.2, 139.1, 138.2, 138.1, 133.0, 132.3, 131.5, 131.2, 131.1, 130.9, 130.8, 130.2, 128.9, 126.9, 126.9, 115.7, 115.5, 115.2, 115.0, 50.9, 24.6, 21.4, 21.1, 16.4, 16.3. FT-IR (cm^{-1}): 2964 (w), 2928 (w), 2901 (w), 1636 (m, $\nu_{C=N}$), 1602 (m), 1474 (s), 1455 (m), 1416 (w), 1359 (m), 1302 (w), 1221 (s), 1157 (s), 1097 (m), 1042 (w), 1016 (m), 936 (w), 867 (w), 832 (s), 798 (m), 751 (w), 726 (m), 688 (w), 655 (w). Anal. calcd for $C_{48}H_{44}F_4N_2$ (724.89): C, 79.53; H, 6.12; N, 3.86%. Found; C, 80.11; H, 6.43; N, 3.80%.

Synthesis of nickel complexes (Ni1–Ni5)

Ni1. Within a Schlenk flask, **L1** (0.11 g, 0.16 mmol) and (DME)$NiBr_2$ (0.05 g, 0.15 mmol) were combined with 10 mL of dichloromethane (DCM). The reaction mixture was vigorously stirred at room temperature for a duration of 12 hours. Following this, 10 mL of anhydrous diethyl ether was introduced to the mixture, prompting the precipitation of the complex. The resulting solid was then washed with diethyl ether and subsequently dried under reduced pressure. This process yielded **Ni1** as a brick-red powder (0.13 g, 90%). FT-IR (cm^{-1}): 2978 (w), 2965 (w), 2908 (w), 1636 (m, $\nu_{C=N}$), 1601 (m), 1569 (m), 1478 (s), 1455 (m), 1412 (w), 1378 (m), 1301 (w), 1221 (s), 1157 (s), 1097 (m), 1040 (w), 1013 (m), 985 (w), 870 (w), 836 (w), 771 (m), 724 (m), 679 (w). Anal calcd for $C_{45}H_{38}Br_2F_4N_2Ni$ (901.31): C, 59.97; H, 4.25; N, 3.11%. Found; C, 59.69; H, 4.52; N, 3.30%.

Ni2. Adopting a synthetic strategy akin to that utilized for the synthesis of **Ni1**, the substitution of **L1** with **L2** led to the formation of **Ni2** as a brick-red powder (0.12 g, 81%). FT-IR (cm^{-1}): 2977 (w), 2960 (w), 2920 (w), 1638 (m, $\nu_{C=N}$), 1602 (m), 1571 (m), 1504 (s), 1445 (m), 1412 (w), 1377 (m), 1333 (w), 1301 (w), 1224 (s), 1127 (s), 1089 (m), 1013 (m), 981 (w), 914 (w), 836 (s), 793 (m), 724 (m), 668 (w). Anal calcd for $C_{47}H_{42}Br_2F_4N_2Ni$ (929.36): C, 60.74; H, 4.56; N, 3.01%. Found; C, 60.55; H, 4.25; N, 3.19%.

Ni3. Adopting a synthetic strategy akin to that utilized for the synthesis of **Ni1**, the substitution of **L1** with **L3** led to the formation of **Ni3** as a brick-red powder (0.11 g, 72%). FT-IR (cm^{-1}): 2965 (w), 2927 (w), 2890 (w), 1639 (m, $\nu_{C=N}$), 1602 (m), 1508 (s), 1457 (m), 1411 (w), 1380 (m), 1325 (w), 1302 (w), 1225 (s), 1158 (s), 1129 (w), 1098 (m), 1057 (m), 1015 (m), 981 (w), 936 (w), 867 (w), 831 (s), 790 (m), 726 (m), 680 (w). Anal calcd for $C_{49}H_{46}Br_2F_4N_2Ni$ (957.42): C, 61.47; H, 4.84; N, 2.93%. Found; C, 61.21; H, 4.52; N, 3.19%.

Ni4. Adopting a synthetic strategy akin to that utilized for the synthesis of **Ni1**, the substitution of **L1** with **L4** led to the formation of **Ni4** as a brick-red powder (0.12 g, 82%). FT-IR (cm^{-1}): 2978 (w), 2922 (w), 2900 (w), 1640 (m, $\nu_{C=N}$), 1601 (m), 1569 (m), 1507 (s), 1455 (m), 1411 (w), 1376 (m), 1301 (w), 1220 (s), 1157 (s), 1120 (w), 1098 (m), 1040 (m), 1013 (m), 938 (w), 835 (s), 788 (m), 724 (m), 679 (w). Anal calcd for $C_{46}H_{40}Br_2F_4N_2Ni$ (915.34): C, 60.36; H, 4.40; N, 3.06%. Found; C, 60.26; H, 5.00; N, 3.19%.

Ni5. Adopting a synthetic strategy akin to that utilized for the synthesis of **Ni1**, the substitution of **L1** with **L5** led to the formation of **Ni5** as a brick-red powder (0.11 g, 73%). FT-IR (cm^{-1}): 2976 (w), 2927 (w), 2868 (w), 1638 (m, $\nu_{C=N}$), 1601 (m), 1569 (m), 1478 (s),1456 (m), 1413 (w), 1377 (m), 1337 (w), 1303 (w), 1217 (s), 1157 (s), 1124 (w), 1098 (m), 1013 (m), 985 (w), 943

(w), 862 (w), 836 (s), 787 (m), 724 (m), 675 (w). Anal calcd for $C_{48}H_{44}Br_2F_4N_2Ni$ (943.39): C, 61.11; H, 4.70; N, 2.97%. Found; C, 61.41; H, 5.10; N, 3.24%.

Author contributions

Dongzhi Zhu, Dedong Jia, and Yanping Ma: methodology, investigation, data curation, original draft preparation, and editing; Qiuyue Zhang: writing, review and editing; Wen-Hua Sun: conceptualization, resources, supervision, funding acquisition, review, and editing.

Conflicts of interest

There are no conflicts to declare.

Data availability

The synthetic procedures for the ligand and nickel complexes are presented in the text along with the analytic data, and related NMR spectra are presented in the SI. The molecular structures and selected bond angles and bond lengths of **Ni1** is presented in the text; the CCDC number, crystal data, and structure refinements are shown in the SI. The detailed data in regard to the catalytic performances of all new nickel complexes appear in the manuscript along with GPC curves and high temperature ^{13}C NMR of representative polyethylenes. More detailed high temperature ^{13}C NMR spectra of polyethylenes appear in the SI. All raw data, such as NMR, GPC, DSC and FT-IR can be obtained upon request from the authors.

CCDC 2452147 contains the supplementary crystallographic data for this paper.[58]

General considerations, general procedure for ethylene polymerization, X-ray crystallographic studies, $^1H/^{13}C$ NMR spectra of monoketone and ligand **L1–L5**, high temperature ^{13}C NMR of polyethylene samples, crystal data and structure refinement for **Ni1**, and references. CCDC 2452147 for **Ni1** complex. For ESI and crystallographic data in CIF or other electronic format. See DOI: **https://doi.org/10.1039/d5ra04501k**.

Acknowledgements

We gratefully acknowledge the financial support by the Strategic Priority Research Program of the Chinese Academy of Sciences (XDC0270101), the Guangxi Natural Science Foundation Program (2025GXNSFBA069499) and the Scientific Research Foundation of Guangxi Minzu University (2023KJQD46).

Notes and references

1 Q. Mahmood and W.-H. Sun, *R. Soc. Open Sci.*, 2018, **5**, 180367.
2 Z. Wang, Q. Liu, G. A. Solan and W.-H. Sun, *Coord. Chem. Rev.*, 2017, **350**, 68–83.
3 X. Li, Z. Hu, Q. Mahmood, Y. Wang, S. Sohail, S. Zou, T. Liang and W.-H. Sun, *Dalton Trans.*, 2024, **53**, 18193–18206.
4 M. A. Khan, Y. Liu, W. Pang, A. Chen and M. Chen, *Chin. J. Chem .*, 2025, **43**, 517–523.
5 J. Yan, B. Lee, S. D. Smith and R. J. Spontak, *Macromol. Rapid Commun.*, 2021, **42**, 2100442.
6 P. Gong, G. Dai, X. Wu, X. Wang, L. Xie, S. Xu and R. Zhong, *The Breast*, 2022, **66**, 317–323.
7 M. A. Wagner, A. Hadian, T. Sebastian, F. Clemens, T. Schweizer, M. Rodriguez-Arbaizar, E. Carreño-Morelli and R. Spolenak, *Addit. Manuf.*, 2022, **49**, 102472.
8 C. Ellingford, H. Smith, X. Yan, C. Bowen, Ł. Figiel, T. McNally and C. Wan, *Eur. Polym. J.*, 2019, **112**, 504–514.
9 K. V. Allahverdiyeva, N. T. Kakhramanov and R. V. Gurbanova, *RSC Adv.*, 2025, **15**, 6541–6563.
10 G. Zanchin and G. Leone, *Prog. Polym. Sci.*, 2021, **113**, 101342.
11 S. Bensason, E. V. Stepanov, S. Chum, A. Hiltner and E. Baer, *Macromolecules*, 1997, **30**, 2436–2444.
12 B. C. Poon, P. Dias, P. Ansems, S. P. Chum, A. Hiltner and E. Baer, *J. Appl. Polym. Sci.*, 2007, **104**, 489–499.
13 F. Deplace, A. K. Scholz, G. H. Fredrickson, E. J. Kramer, Y.-W. Shin, F. Shimizu, F. Zuo, L. Rong, B. S. Hsiao and G. W. Coates, *Macromolecules*, 2012, **45**, 5604–5618.
14 K. S. O'Connor, A. Watts, T. Vaidya, A. M. LaPointe, M. A. Hillmyer and G. W. Coates, *Macromolecules*, 2016, **49**, 6743–6751.
15 H. Ohtaki, F. Deplace, G. D. Vo, A. M. LaPointe, F. Shimizu, T. Sugano, E. J. Kramer, G. H. Fredrickson and G. W. Coates, *Macromolecules*, 2015, **48**, 7489–7494.
16 C. Wu, M. Ren, L. Hou, S. Qu, X. Li, C. Zheng, J. Chen and W. Wang, *Engineering*, 2023, **30**, 93–99.
17 F. Li and W. Liu, *Can. J. Chem. Eng.*, 2023, **101**, 4992–5019.
18 G. Yang, Z. Zhang, Z. Ma, C. Li and C. Zou, *Polymer*, 2024, **294**, 126699.
19 F. Li, Y. Bai, J. He, T. Song, W. Gao, X. Mu and Y. Mu, *Macromolecules*, 2023, **56**, 6764–6775.
20 Y.-B. Wang, C. Nan, W. Zhuo, C. Zou, H. Jiang, X.-Q. Hao, C. Chen and M.-P. Song, *Inorg. Chem.*, 2023, **62**, 5105–5113.
21 T. Wang, C. Wu, X. Ji and D. Cui, *Angew. Chem., Int. Ed.*, 2021, **60**, 25735–25740.
22 A. L. N. Da Silva, M. C. G. Rocha, F. M. B. Coutinho, R. Bretas and C. Scuracchio, *J. Appl. Polym. Sci.*, 2000, **75**, 692–704.
23 L. K. Johnson, C. M. Killian and M. Brookhart, *J. Am. Chem. Soc.*, 1995, **117**, 6414–6415.
24 C. M. Killian, D. J. Tempel, L. K. Johnson and M. Brookhart, *J. Am. Chem. Soc.*, 1996, **118**, 11664–11665.
25 G. W. Son, K. B. Bijal, D.-W. Park, C.-S. Ha and I. Kim, *Catal. Today*, 2006, **111**, 412–416.
26 X. Yan, Z. Fu, Y. Li and Y. Shi, *Polym. Bull.*, 2012, **68**, 327–339.
27 Z. Dong and Z. Ye, *Polym. Chem.*, 2012, **3**, 286–301.
28 I. Pierro, G. Zanchin, E. Parisini, J. Martí-Rujas, M. Canetti, G. Ricci, F. Bertini and G. Leone, *Macromolecules*, 2018, **51**, 801–814.
29 N. Zhu, M. A. Khan, W. Pang, S. Behzadi and M. Qasim, *Eur. Polym. J.*, 2022, **178**, 111497.

30 I. D'Auria, M. Maggio, G. Guerra and C. Pellecchia, *Macromolecules*, 2017, **50**, 6586–6594.
31 S.-Y. Chen, R.-C. Pan, Y. Liu and X.-B. Lu, *Organometallics*, 2021, **40**, 3703–3711.
32 A. E. Cherian, J. M. Rose, E. B. Lobkovsky and G. W. Coates, *J. Am. Chem. Soc.*, 2005, **127**, 13770–13771.
33 Q. Mahmood, Z. Hu, G. Ren and W.-H. Sun, *Coord. Chem. Rev.*, 2025, **541**, 216833.
34 H. Liu, W. Zhao, X. Hao, C. Redshaw, W. Huang and W.-H. Sun, *Organometallics*, 2011, **30**, 2418–2424.
35 R. Wu, Y. Wang, R. Zhang, C.-Y. Guo, Z. Flisak, Y. Sun and W.-H. Sun, *Polymer*, 2018, **153**, 574–586.
36 Q. Mahmood, Y. Zeng, E. Yue, G. A. Solan, T. Liang and W.-H. Sun, *Polym. Chem.*, 2017, **8**, 6416–6430.
37 X. Wang, L. Fan, Y. Ma, C.-Y. Guo, G. A. Solan, Y. Sun and W.-H. Sun, *Polym. Chem.*, 2017, **8**, 2785–2795.
38 S. Kong, C.-Y. Guo, W. Yang, L. Wang, W.-H. Sun and R. Glaser, *J. Organomet. Chem.*, 2013, **725**, 37–45.
39 L. Fan, S. Du, C. Y. Guo, X. Hao and W.-H. Sun, *J. Polym. Sci., Part A: Polym. Chem.*, 2015, **53**, 1369–1378.
40 Q. Mahmood, Y. Zeng, X. Wang, Y. Sun and W.-H. Sun, *Dalton Trans.*, 2017, **46**, 6934–6947.
41 M. Liu, R. Zhang, Y. Ma, M. Han, G. A. Solan, W. Yang, T. Liang and W.-H. Sun, *Polym. Chem.*, 2022, **13**, 1040–1058.
42 S. Du, S. Kong, Q. Shi, J. Mao, C. Guo, J. Yi, T. Liang and W.-H. Sun, *Organometallics*, 2015, **34**, 582–590.
43 R. Wu, Y. Wang, L. Guo, C. Y. Guo, T. Liang and W.-H. Sun, *J. Polym. Sci., Part A: Polym. Chem.*, 2018, **57**, 130–145.
44 Q. Zhang, R. Zhang, Y. Ma, G. A. Solan, T. Liang and W.-H. Sun, *Appl. Catal., A*, 2019, **573**, 73–86.
45 Y. Wang, A. Vignesh, M. Qu, Z. Wang, Y. Sun and W.-H. Sun, *Eur. Polym. J.*, 2019, **117**, 254–271.
46 X. Wang, L. Fan, Y. Yuan, S. Du, Y. Sun, G. A. Solan, C.-Y. Guo and W.-H. Sun, *Dalton Trans.*, 2016, **45**, 18313–18323.
47 R. Zhang, Z. Wang, Y. Ma, G. A. Solan, Y. Sun and W.-H. Sun, *Dalton Trans.*, 2019, **48**, 1878–1891.
48 D. Zhu, D. Jia, Q. Zhang, Y. Ma, Q. Mahmood and W.-H. Sun, *Molecules*, 2025, **30**, 1847.
49 D. Jia, W. Zhang, W. Liu, L. Wang, C. Redshaw and W.-H. Sun, *Catal. Sci. Technol.*, 2013, **3**, 2737–2745.
50 X. Li, L. Qin, Q. Mahmood, Z. Yu, S. Zou, Y. Wang, T. Liang and W.-H. Sun, *Eur. Polym. J.*, 2023, **200**, 112520.
51 Q. Liu, W. Zhang, D. Jia, X. Hao, C. Redshaw and W.-H. Sun, *Appl. Catal. A Gen.*, 2014, **475**, 195–202.
52 W. Yang, J. Yi and W.-H. Sun, *Macromol. Chem. Phys.*, 2015, **216**, 1125–1133.
53 G. B. Galland, R. F. de Souza, R. S. Mauler and F. F. Nunes, *Macromolecules*, 1999, **32**, 1620–1625.
54 Y. Zheng, S. Jiang, M. Liu, Z. Yu, Y. Ma, G. A. Solan, W. Zhang, T. Liang and W.-H. Sun, *RSC Adv.*, 2022, **12**, 24037–24049.
55 V. Rosa, T. Avilés, G. Aullon, B. Covelo and C. Lodeiro, *Inorg. Chem.*, 2008, **47**, 7734–7744.
56 K. V. Vasudevan, M. Findlater and A. H. Cowley, *Chem. Commun.*, 2008, **16**, 1918–1919.
57 D. Zhang, E. T. Nadres, M. Brookhart and O. Daugulis, *Organometallics*, 2013, **32**, 5136–5143.
58 D. Zhu, Q. Zhang, D. Jia, Y. Ma and W.-H. Sun, CCDC 2452147: Experimental Crystal Structure Determination, 2025, DOI: **10.5517/ccdc.csd.cc2n9nj5**.